Steady regime of radiation pressure acceleration with foil thickness adjustable within micrometers under a 10–100 PW laser

Meng Liu [1,3] Wei-Min Wang [2,4,*] and Yu-Tong Li [1,5,6,†]

[1] *Beijing National Laboratory for Condensed Matter Physics, Institute of Physics, CAS, Beijing 100190, China*
[2] *Department of Physics and Beijing Key Laboratory of Opto-electronic Functional Materials and Micro-nano Devices, Renmin University of China, Beijing 100872, China*
[3] *Department of Mathematics and Physics, North China Electric Power University, Baoding, Hebei 071003, China*
[4] *Key Laboratory of Quantum State Construction and Manipulation (Ministry of Education), Renmin University of China, Beijing 100872, China*
[5] *School of Physical Sciences, University of Chinese Academy of Sciences, Beijing 100049, China*
[6] *Songshan Lake Materials Laboratory, Dongguan, Guangdong 523808, China*

(Received 14 February 2023; accepted 18 December 2023; published 26 January 2024)

Quasimonoenergetic GeV-scale protons are predicted to be efficiently generated via radiation pressure acceleration (RPA) when the foil thickness is matched with the laser intensity, e.g., L_{mat} of several nm to 100 nm for $10^{19}-10^{22}\,\mathrm{W\,cm^{-2}}$ available in laboratory. However, nonmonoenergetic protons with much lower energies than predicted were usually observed in RPA experiments because of too small foil thickness which cannot support insufficient laser contrast and foil surface roughness. Besides the technical problems, we here find that there is an upper-limit thickness L_{up} derived from the requirement that the laser energy should dominate over the ion source energy in the effective laser-proton interaction zone, and L_{up} is lower than L_{mat} with the intensity below $10^{22}\,\mathrm{W\,cm^{-2}}$, which causes inefficient or unsteady RPA. As the intensity is enhanced to $\geqslant 10^{23}\,\mathrm{W\,cm^{-2}}$ provided by 10–100 PW laser facilities, L_{up} can significantly exceed L_{mat}, and therefore RPA becomes efficient. In this regime, L_{mat} acts as a lower-limit thickness for efficient RPA, so the matching thickness can be extended to a continuous range from L_{mat} to L_{up}; the range can reach micrometers, within which foil thickness is adjustable. This makes RPA steady and meanwhile the above technical problems can be overcome. Particle-in-cell simulation shows that multi-GeV quasimonoenergetic proton beams can be steadily generated and the fluctuation of the energy peaks and the energy conversation efficiency remains stable although the thickness is taken in a larger range with increasing intensity. This work predicts that near future RPA experiments with 10–100 PW facilities will enter a new regime with a large range of usable foil thicknesses that can be adjusted to the interaction conditions for steady acceleration.

DOI: 10.1103/PhysRevE.109.015208

I. INTRODUCTION

Laser plasma interaction can provide approaches to realize compact ion acceleration due to high acceleration gradients [1–3]. The achieved ion beams with short bunch duration, compact size, and high density can be applied in fundamental science, plasma diagnostics, and medicine [1,2,4]. One of the most attracting applications, tumor therapy [5,6] demands proton beams with energy above 200 MeV and energy spread below 1% [1,2]. Varieties of ion acceleration schemes have been proposed with the advancements in both high-power laser technology and targetry in the past two decades [7–15]. Among them, target normal sheath acceleration (TNSA) [16] is the predominant mechanism in most experiments of ion acceleration. TNSA demonstrated cut-off proton energies near 100 MeV [11,12], but the corresponding spectra are usually broad and the number of protons at the cut-off energy is small. Radiation pressure acceleration (RPA) [17–21] is predicted to generate high-energy quasimonoenergetic ion beams with a sufficient number of protons in the monoenergetic peak, which has potential to meet the requirements of the key applications mentioned above.

However, RPA experiments usually achieved nonmonoenergetic proton beams or quasimonoenergetic peaks at much lower energies than theoretical predictions [22–24]. In RPA, the radiation pressure of an intense circularly polarized (CP) laser pulse can push a substantial number of electrons forward, resulting in a strong charge-separation field for ion acceleration. When the radiation pressure is balanced with the charge-separation force, continuous ion acceleration can be obtained, which presents a matched foil thickness [2,21]

$$L_{\mathrm{mat}} \simeq \frac{a_0 n_c \lambda}{\pi n_e}, \tag{1}$$

where $a_0 = (\frac{I_0\lambda^2}{2.74\times10^{18}\,\mathrm{W\,cm^{-2}\mu m^2}})^{1/2}$ is the normalized laser amplitude in the case of circular polarization, $n_c = \frac{m_e\omega^2}{4\pi e^2}$ is the critical density, and I_0, ω, and λ are the laser

*weiminwang1@ruc.edu.cn
†ytli@iphy.ac.cn

intensity, frequency, and wavelength, respectively. For $10^{19}-10^{22}\,\mathrm{W\,cm^{-2}}$ used in the existing RPA experiments [22,25–29], L_{mat} is at a few nm to 100 nm. With such small thicknesses, the foil is easy to be deformed or broken by the amplified spontaneous emission (ASE) and prepulse of the high-power laser pulse [30,31] before the main pulse interaction with the foil. Furthermore, according to the present target fabrication technology, the surface roughness is typically of the same order with such thickness. These limitations in the current target and laser technology tend to result in inefficiency and unsteadiness of RPA, which could become worse due to transverse instabilities [32–34] and plasma heating [35].

Besides the above factors, we find here that there is an upper-limit thickness L_{up} for efficient RPA and L_{up} is lower than or around L_{mat} with the intensity below $10^{22}\,\mathrm{W\,cm^{-2}}$ ($a_0 = 61$) adopted in reported experiments [22,25–27], which could cause inefficient or unsteady acceleration. As the intensity is enhanced to $10^{23}\,\mathrm{W\,cm^{-2}}$, made available recently [36], L_{up} starts to significantly exceed L_{mat}, resulting in that the matching thickness can be extended to a large range from L_{mat} to L_{up} and up to several micrometers. This can bring both efficient and steady RPA and meanwhile the above technical problems can be overcome. The upper-limit thickness and the enlarging thickness range for increasing laser intensity are discussed in detail in Sec. II; then we perform multidimensional PIC simulations in Sec. III to verify the existing requirement of the driving laser energy dominating over the proton energy in the effective laser-proton interaction zone. In this regime, multi-GeV quasimonoenergetic proton beams can be steadily generated and the fluctuation of the energy peaks and the energy conversation efficiency remains stable although the thickness is taken in a larger range with increasing intensity. We also check the influence of the strong field quantum electrodynamics (QED) effects and the foil composition for efficient RPA at the end.

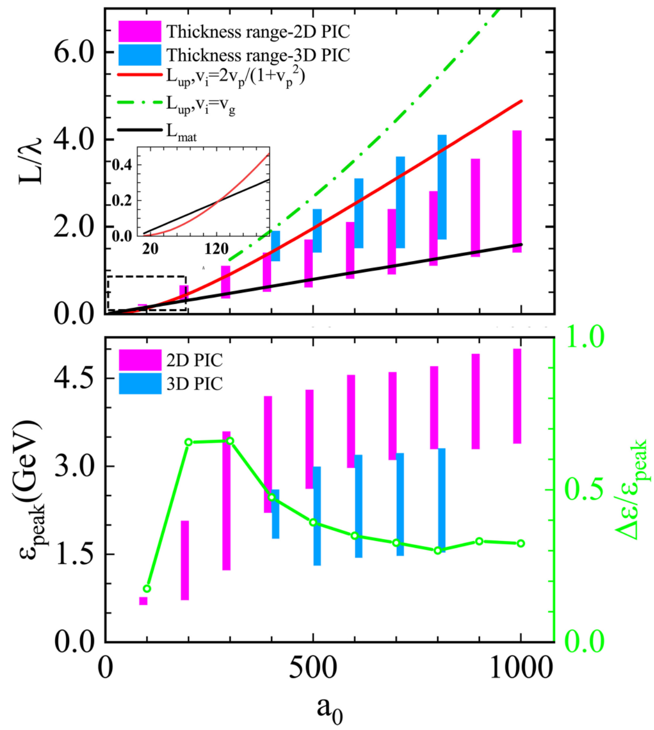

FIG. 1. (a) The target thickness L for efficient RPA as a function of the laser amplitude a_0, where the pink rectangles and blue rectangles correspond to 2D and 3D PIC results, respectively, the black line is L_{mat} calculated from Eq. (1), and the red and green dashed lines show L_{up} calculated from Eq. (2) with v_i estimated as $\frac{2v_p}{1+v_p^2}$ and v_g, respectively. The target thickness for efficient RPA is counted when a quasimonoenergetic proton beam is generated in PIC simulation. (b) The corresponding energy peaks $\varepsilon_{\mathrm{peak}}$ of the quasimonoenergetic proton beams are displayed by pink rectangles and blue rectangles for 2D and 3D PIC results, respectively. The green line with circles is the fluctuation of the peak energies $\frac{\Delta\varepsilon}{\varepsilon_{\mathrm{peak}}}$ obtained from the 2D-PIC simulations.

II. THE UPPER-LIMIT THICKNESS FOR STEADY RPA

We consider that laser intensity of $10^{22}-10^{23}\,\mathrm{W\,cm^{-2}}$ and the generated proton beam can achieve several GeV energy with the velocity approaching the light speed c after it experiences the first acceleration stage of tens of fs with a typical piston velocity, as will be shown in Fig. 2. During the acceleration process, the proton rest energy is important in the first stage and it is gradually dominated by the kinetic energy. Therefore, both the rest and kinetic energy is needed to consider in our case, i.e., $W_R \geqslant n_i L\pi R^2(E_k + m_i c^2) = n_i L\pi R^2\gamma m_i c^2$ for the steady RPA, where W_R is the laser energy within the focal spot radius R and the foil thickness is L, n_i is the ion density, and $m_i c^2$ is the ion rest energy. Note that Daido *et al.* [1] gave $W_R \geqslant n_i L\pi R^2\gamma m_i c^2 \simeq n_i L\pi R^2 m_i c^2$ by use of that the laser energy should be much larger than the total ion rest energy, which is suitable for low-energy ion acceleration. Esikepov *et al.* and Bulanov S.V. *et al.* considered that kinetic energy is dominant for high-energy ion acceleration and presented final ion energy $E_{i,\max} \sim \frac{W_R}{n_i L\pi R^2}$ [17,37]. In our case, the requirement that the driving laser energy should dominate over the ion rest and kinetic energy within the laser focal spot gives the upper limit thickness

$$L_{\mathrm{up}} \leqslant \frac{W_R\sqrt{1-v_i^2/c^2}}{\pi R^2 n_i m_i c^2}, \tag{2}$$

so that the laser pulse has enough surplus energy to transform to the ions kinetic energy, independent of the acceleration process. Here, the full laser pulse length is taken to calculate the laser energy and the proton relativistic kinetic energy has been taken as $E_k = (\gamma-1)m_i c^2 = (\frac{1}{\sqrt{(1-v_i^2/c^2)}}-1)\,m_i c^2$. In the RPA scheme, we can estimate the ion velocity v_i as $\frac{2v_p}{1+v_p^2}$, where $v_p = \frac{\sqrt{\Pi}}{1+\sqrt{\Pi}}$ is the piston velocity in the relativistic case [17,38–40], and $\Pi = \frac{2a_0^2 Z n_c m_e}{A n_e m_i}$, $\frac{Z}{A}$ is the charge-mass ratio, and m_i is the ion mass. Once the ions are continuously accelerated to relativistic velocity, the final ion velocity should be estimated as the relativistic group velocity of the laser v_g [15,38]. Here $v_g \simeq (1-\frac{n_e}{n_{cr}})^{1/2}c$ and $n_{cr} \simeq (1+0.5a_0^2)^{1/2}n_c$ is the relativistic critical density for CP pulses at normalized amplitudes $a_0 \gg 1$ [38]. Our simulations below will show that they are two typical velocities in

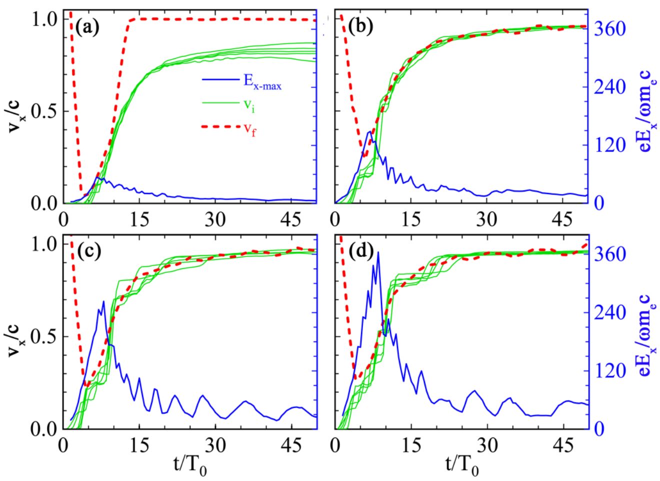

FIG. 2. Temporal evolution of the laser wavefront velocity v_f (red dotted line) and tracked proton velocity v_i (green line), where we track 100 protons gaining high energies finally and take five typical ones. Evolution of the maximum of the longitudinal electric field $E_{x-\max}$ (corresponding to the right y axis) is also displayed by the blue line. Here the laser amplitude a_0 and target thickness L are taken as (100, 0.18λ), (300, 0.56λ), (500, 1.1λ), and (700, 1.7λ) in (a)–(d), respectively.

the "hole-boring" [19,41] and the "light-sail" [14,15,42–44] phases in ion acceleration, respectively.

According to Eqs. (1) and (2) with a given density $n_e = 200n_c$, we calculate $L_{\rm mat}$ from Eq. (1) and plot it by the black line in Fig. 1(a), and calculate $L_{\rm up}$ from Eq. (2) with v_i estimated as $\frac{2v_p}{1+v_p^2}$ or v_g and show them by the red and green dashed lines in Fig. 1(a). Here the total laser energy W_R within the focal spot radius R can be calculated when a $30fs$ laser pulse with the given intensity profile of $I(t,y) = I_0 exp(-\frac{2t^2}{\tau^2})exp(-\frac{y^4}{R^4})$ propagates in vacuum and I_0 is the peak intensity of the initial laser pulse. $L_{\rm up} = L_{\rm mat} = 0.196\lambda$ when $a_0 = 122$ (corresponding to $4\times10^{22}\,{\rm W\,cm^{-2}}$); and $L_{\rm up} > L_{\rm mat}$ always holds for $a_0 > 122$, as shown in Fig. 1(a). Note that the intensities below and far below $4\times10^{22}\,{\rm W\,cm^{-2}}$ were adopted in existing RPA experiments [22,26,27]. Therefore, unsteady experimental results are not only because of the too small thickness $L_{\rm mat}$ with low tolerance to the insufficient laser contrast and foil surface roughness, but also because of the requirement that the driving laser energy should dominate over the ion source energy within the laser focal spot and the effective plasma thickness, i.e., the thickness L should be less than $L_{\rm up}$. Adopting L as $L_{\rm mat}$ for efficient RPA has been widely recognized, so the requirement of $L_{\rm up} > L$ is roughly equivalent to $L_{\rm up} > L_{\rm mat}$. As the laser intensity is higher than $4\times10^{22}\,{\rm W\,cm^{-2}}$, an efficient RPA with $L_{\rm up} > L_{\rm mat}$ starts to be possible. Furthermore, to achieve a steady RPA, $L_{\rm up}$ should be much greater than $L_{\rm mat}$ and then the thickness can be chosen in a large range. For example, when $a_0 = 300$ (corresponding to $2.47\times10^{23}\,{\rm W\,cm^{-2}}$), $L_{\rm up} = 0.91\lambda$ and $L_{\rm mat} = 0.48\lambda$ and, in principle, the thickness can be taken in a range from 0.48λ to 0.91λ. For higher laser intensities, the thickness range $\Delta L = L_{\rm up} - L_{\rm mat}$ is enlarged further, which can be observed in Fig. 1(a) and also explained in the following.

Besides, one can easily derive $L_{\rm up} \propto \frac{\xi^2\sqrt{1+2\alpha_0\xi}}{1+\alpha_0\xi}$ and $L_{\rm mat} \propto \xi\sqrt{\frac{n_c}{n_e}}$ from Eqs. (1) and (2), where $\alpha_0 = \frac{\sqrt{2}Zm_e}{Am_i}$ and $\xi = a_0\sqrt{\frac{n_c}{n_e}}$. For a given n_e or foil species, $L_{\rm up}$ increases more quickly than $L_{\rm mat}$ with the growth of a_0, i.e., the thickness range ΔL is enlarged continuously. These analytical results are verified by our particle-in-cell (PIC) simulation results shown by the pink and blue rectangles in Fig. 1(a).

III. PIC SIMULATION RESULTS

We perform two-dimensional (2D) and three-dimensional (3D) PIC simulations with the EPOCH code [45]. For 2D PIC, a CP laser pulse with a wavelength $\lambda = 1\mu$m and an intensity profile of $I_0 \exp(-2t^2/\tau^2)\exp(-y^4/R^4)$ is incident along the x direction, where the spot radius is $R = 6\lambda$ and the duration is 30 fs. The pulse arrives at the vacuum-foil interface $x = 15\lambda$ at $t = 0$. The foil is composed of protons H^+ and e^- with $n_e = 200n_c$. We take a simulation box $40\lambda \times 50\lambda$ (4000×2500 cells in $x \times y$) moving along the x direction at the speed of light and each cell has 100 macroparticles in the foil region. Besides, we use the same laser pulse and foil composition in 3D PIC simulations. We take a simulation box $40\lambda \times 30\lambda \times 30\lambda$ divided into $1200 \times 900 \times 900$ cells in $x \times y \times z$ and the box is moving along the x direction at the speed of light. Each cell has 100 macroparticles in the foil region.

Figure 1(a) shows the target thickness for efficient RPA as a function of a_0, where the pink rectangles and blue rectangles correspond to 2D and 3D PIC results, respectively. For a given a_0, we change the foil thickness and count the thickness value with which a quasimonoenergetic GeV proton beam is generated (see Note 1 and Fig. S1 of the Supplemental Material [46]). Then the counted values are illustrated by the rectangles representing adjustable thickness ranges. One can see that the range is enlarged with the growth of a_0 and the pink rectangles fall well between the black and red lines, in good agreement with Eqs. (1) and (2). This suggests that there is indeed an upper-limit thickness for efficient RPA, set by the requirement of the driving laser energy dominating over the proton energy within the laser focal spot and the effective plasma thickness.

The PIC results also indicate that the well-known matching thickness $L_{\rm mat}$ acts as a lower-limit value for efficient RPA, and then the matching thickness originally used as an isolated value point can be extended to a continuous range. This is because $L_{\rm mat}$ is derived under an ideal condition that the foil electrons as a whole are pushed forward and form a charge-separation field to balance with the laser radiation pressure exerted on the electrons. Actually, only part of the foil electrons can be pushed forward out of the foil, which becomes more significant for a relatively large thickness with high laser intensity. Furthermore, the electrostatic pressure of charge-separation field $E_x e n_{p0} l_s$ [21] should be higher than the radiation pressure $\frac{2I}{c}$, where $n_{p0}l_s \simeq n_e L$ and the charge-separation field $E_x = 4\pi e n_e L$. Otherwise, the foil electrons can be blown out, the compressed electron layer cannot be formed, and ions cannot be accelerated.

Hence,

$$L \geqslant L_{\mathrm{mat}} \tag{3}$$

should be a more reasonable condition for sustaining the charge-separation field to accelerate ions continuously. It should be noted that Eqs. (1) and (2) are given in the 1D case. The omitted transverse effects, e.g., thermal expansion induced by the strong electron heating and transverse instabilities [32–35], tend to deteriorate the target and a thicker foil is needed to overcome the deterioration. Thus, the effective foil thickness ranges from 3D PIC simulations [blue rectangles in Fig. 1(a)] do not fall well between the black and red lines in Fig. 1(a) and are higher than those in 2D PIC results because of the transverse effects. On the other hand, the whole energy of the laser pulse cannot be used to accelerate the foil in reality. In 2D PIC simulations, the proton relativistic velocity, estimated as the laser relativistic group velocity v_g, grows slowly since $a_0 \geqslant 300$, and the energy conversion efficiency from the laser pulse to the kinetic protons maintains around 20%–25% (See Table S1 of the Supplemental Material [46]). Moreover, the reflected laser energies are about 9.5% and 7.2%, respectively, for the cases with $= 300$ and $a_0 = 500$ in Fig. 2. Thus, the effective foil thickness ranges in 2D simulations are lower than the prediction values from Eq. (2).

The enlarged effective thickness range bounded by L_{mat} and L_{up} provides a favorable freedom for foil thickness choice and the matched thickness can be adopted as a value much higher than the original prediction by L_{mat}. For instance, quasimonoenergetic GeV proton beams can be stably generated from the foil with a thickness within 0.4λ–1.2λ for $a_0 = 300$, and 0.8λ–2.1λ for $a_0 = 600$ from PIC results (also see Note 1 and Fig. S1 of the Supplemental Material [46]). When $a_0 \geqslant 1000$, the thickness range ΔL even enlarges above 2λ, favoring the target design in future experiments.

Although the thickness is taken in a larger range with increasing a_0, the fluctuation of the energy peaks remains stable, as shown in Fig. 1(b). This figure plots the energy peaks $\varepsilon_{\mathrm{peak}}$ of the quasimonoenergetic proton beams obtained from 2D and 3D PIC results. In the typical simulation with $a_0 = 300$, the peak energy decreases from 3.6 GeV to 1.2 GeV as the foil thickness increases from 0.4λ to 1.2λ. With a larger amplitude $a_0 = 600$, the peak energy only decreases from 4.5 GeV to 3.0 GeV as the foil thickness increases from 0.8λ to 2.1λ (also see Note 1 and Fig. S1 of the Supplemental Material [46]). The green line in Fig. 1(b) displays the energy fluctuation $\frac{\Delta\varepsilon}{\varepsilon_{\mathrm{peak}}}$ as a function of a_0. It is shown it reaches 70% at $a_0 = 200$, decreases to 40%, and then maintains around this value since $a_0 > 400$. Even when the thickness range ΔL is above 2λ with $a_0 \geqslant 1000$, $\Delta\varepsilon/\varepsilon_{\mathrm{peak}}$ does not grow. This is because the proton velocity or peak energy is mainly determined by the laser relativistic group velocity which increases slowly with the growing a_0 when a_0 is sufficiently large. The slowly increasing group velocity also causes the energy conversion efficiency of the protons to basically remain around 20%–25% as shown in the Note 2, Fig. S3, and Table S1 of the Supplemental Material [46].

Figure 2 shows the evolution of tracked proton velocity v_i and the laser wavefront velocity v_f representing the group velocity, where v_f is defined as the velocity of the surface where

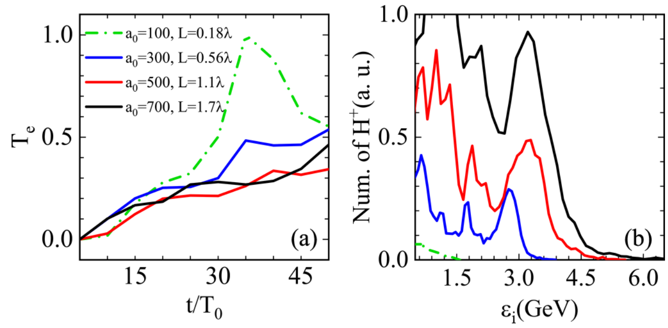

FIG. 3. (a) Evolution of the plasma electron temperature and (b) the energy spectra of protons at $t = 70T_0$, where different lines in (a) and (b) represent different (a_0, L) corresponding to the parameters taken in Figs. 2(a)–2(d), respectively. The plasma temperatures are calculated with the electrons in the compressed density layer and normalized by that in the case of $a_0 = 100$.

the laser intensity is $\frac{I_0}{100}$ [47], corresponding to the laser normalized amplitude of $\frac{a_0}{10}$. The evolution of v_f can be separated into two stages in Figs. 2(b)–2(d). In the first stage with $t \lesssim 11 - 12T_0$, v_f first decreases dramatically at the beginning of the interaction of the laser with the foil, and later increases quickly along with the foil being pushed forward by laser radiation pressure. This stage has been widely studied [19,40] and v_i can be estimated as $\frac{2v_p}{1+v_p^2}$. At the second stage after about $12T_0$, v_f becomes roughly constant and v_i is very close to v_f in Figs. 2(b)–2(d) with $a_0 = 300 - 700$, meaning that the protons are efficiently and continuously accelerated and then move along with the laser pulse. In this stage, v_i can be estimated by the relativistic group velocity v_g [15,32,48], where $v_i \simeq 0.973c$ and $v_i \simeq 0.982c$ for the cases with $a_0 = 500$ and $a_0 = 700$ read from Figs. 2(c) and 2(d). In this case, the group velocity $v_g \simeq (1 - \frac{n_e}{\sqrt{2}a_0 n_c})c$ grows slowly with a_0 ($a_0 \gg 1$). This agrees with Fig. 1(b) that the peak energy increases slowly from $a_0 = 400$ to $a_0 = 1000$. By contrast, in Fig. 2(a) with $a_0 = 100$, the protons velocity can only reach $0.75c$ much lower than v_f because the laser wavefront breaks through the foil and the protons cannot catch up.

Figure 3 shows that the plasma heating is suppressed with the growing laser intensity, facilitating the acceleration. Compared with the case with $a_0 = 100$, the plasma temperature is reduced by 50% with $a_0 = 300$, and 75% with $a_0 = 500$ and 700 at the second stage. In efficient RPA at high intensities, the protons and electrons move along with the laser pulse and then their velocities [see Figs. 2(b)–2(d)] are close to c and mainly in the longitudinal direction, i.e., most of the particle energies are longitudinal, and the protons cover the majority of the energies. This causes significant reductions of the temperature and the transverse spread of electrons. The upper-limit thickness L_{up} in Eq. (2) is given by the requirement that the driving laser energy within the full pulse length should dominate over the proton source energy within the full foil thickness during the efficient RPA. The requirement is verified by Figs. 4(a2)–4(d2), which displays the laser energy [red curve of Figs. 4(a2)–4(d2)] and the protons energy [blue curve of Figs. 4(a2)–4(d2)] by integrating the energy density of the laser pulse and the protons [Figs. 4(a1)–4(d1)], respectively,

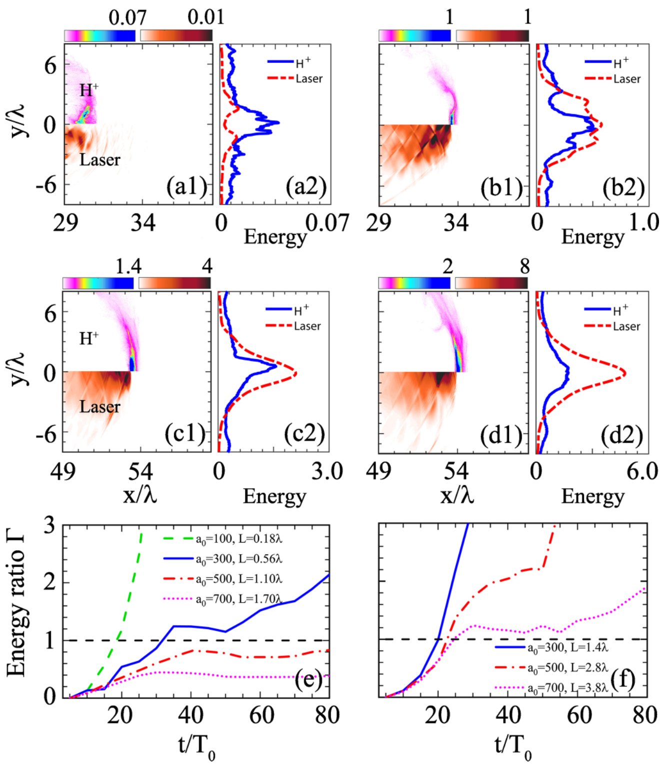

FIG. 4. (a1)–(d1) Spatial distributions of energy densities of the protons (top half) and the laser (bottom half); the laser energy and the ion energy integrated over the same longitudinal space are also plotted by the red curve and blue curve of the subfigures (a2)–(d2), respectively, where (a) and (b) are the cases with $a_0 = 100/300$ at $t = 30T_0$, and (c) and (d) are the cases with $a_0 = 500/700$ at $t = 50T_0$. The units of the color scales are normalized by the energy density in the case with $a_0 = 300$. (e), (f) Temporal evolution of the energy ratio between the protons and the laser, where the ratio is calculated by the energy peaks of the protons and the laser.

over the same longitudinal space. We calculate the laser energy by integrating over the effective pulse length (except the reflected laser energy) and the ion energy by integrating over the effective plasma thickness, e.g., in Fig. 4(c1) the effective laser pulse length is about 4.5λ (from 49.0λ to 53.5λ) and the effective plasma thickness is about 0.8λ (from 53.1λ to 53.9λ) When the thickness is in the range from $L_{\rm mat}$ to $L_{\rm up}$ for efficient RPA, e.g., Figs. 4(b)–4(d), the laser energy is dominant over the proton energy. Figure 4(e) illustrates the evolution of the energy ratio Γ of the protons to the laser. Γ is less than one in the whole simulation duration for $(a_0, L) = (500, 1.1\lambda)$ and (700, 1.7λ) and before $t = 30T_0$ for (300, 0.56λ) [also see Fig. 4(b) given at $t = 30T_0$], which corresponds to the efficient acceleration time. While the thickness is larger than $L_{\rm up}$ for the given $a_0 = 300$, 500, and 700, shown in Fig. 4(f), Γ starts to be more than one as early as about $t = 20T_0$ and the acceleration is inefficient (i.e., no quasimonoenergetic peak or much lower peak energy).

IV. CONCLUSION AND DISCUSSION

In summary, we have found there is an upper-limit thickness $L_{\rm up}$ for efficient RPA, deriving from the requirement that the driving laser energy should dominate over the proton source energy within the laser focal spot and the effective plasma thickness. The well-known matching thickness $L_{\rm mat}$ acts as a lower-limit value, and therefore, the matching thickness originally used as an isolated value point can be extended to a continuous range from $L_{\rm mat}$ to $L_{\rm up}$. $L_{\rm up} > L_{\rm mat}$ can be achieved for steady RPA with $I_0 > 4 \times 10^{22}$ W cm^{-2} and the thickness range $L_{\rm up} - L_{\rm mat}$ is enlarged with the laser intensity. For $10^{23} \sim 10^{24}$ W cm^{-2} delivered from the 10 PW and 100 PW laser facilities [49–51], the thickness range can reach a few micrometers providing favorable freedom for foil thickness choice in RPA experiments. Although the thickness is taken in a larger range with increasing intensity, the fluctuation of the energy peaks as well as the energy conversation efficiency remain stable. This work predicts that near future RPA experiments with 10–100 PW laser facilities will enter a new regime with a large-range of usable foil thicknesses that can be adjusted to the interaction conditions for steady ion acceleration.

Note that in Eq. (2) the proton velocity v_i is mainly estimated by the laser relativistic group velocity v_g, which has been verified by Fig. 2, and the laser energy is calculated with the spot radius at the focusing plane, which does not change significantly with laser propagation within the Rayleigh length (113 μm in our case). Therefore, Eq. (2) can give a reasonable $L_{\rm up}$ close to the PIC simulations.

We also check the influence of the strong field quantum electrodynamics (QED) effects [52–55] on RPA. The influence enhances with the growing a_0, but basically it can be negligible (see Note 3 and Fig. S4 of the Supplemental Material [46]). With $a_0 = 1000$, the energy conversion efficiency of the γ photons increases with the target thickness and it reaches 8% at the maximum thickness 4.4λ for efficient RPA, where both the energy peak and energy conversion of the protons are reduced by less than 6%. In efficient RPA, electrons move mainly along the laser propagating direction which makes small QED parameters and weak QED effects [55,56]. For the laser pulse at intensity of $10^{22} - 10^{24}$ W cm^{-2} in our simulations, the preplasma produced by ASE should not significantly influence the generation of the quasimonoenergetic ion beams according to the discussion in Refs. [57,58], because the preplasma is relativistically underdense and therefore can be ignored. As the intensity exceeds 10^{25} W cm^{-2}, the QED cascades could be triggered in the preplasma and it starts to become opaque for the laser, where the QED effects could dominate the classically relativistic transparency and laser hole boring [59].

Besides the foil species composed of $n_H = n_e = 200n_c$, we also investigated the steady RPA process for the lower density with $n_H = n_e = 100n_c$ (see Table S1 in the Supplemental Material [46]). Moreover, the realistic targets, lithium hydride (LiH) [60] with different thicknesses, are also adopted and the results agree with Eq. (2) (see Note 4 and Fig. S5 of the Supplemental Material [46]).

ACKNOWLEDGMENTS

This work was supported by the National Key R&D Program of China (Grant No. 2018YFA0404801), National Natural Science Foundation of China (Grants No. 12205366 and No. 11775302), the Strategic Priority Research Program of Chinese Academy of Sciences (Grants No. XDA25050300 and No. XDA25010300), the Fundamental Research Funds for the Central Universities (Grant No. 2020MS138), and the Fundamental Research Funds for the Central Universities, the Research Funds of Renmin University of China (20XNLG01). Computational resources have partially been provided by the Physical Laboratory of High Performance Computing at Renmin University of China.

[1] H. Daido, M. Nishiuchi, and A. S. Pirozhkov, Review of laser-driven ion sources and their applications, Rep. Prog. Phys. **75**, 056401 (2012).

[2] A. Macchi, M. Borghesi, and M. Passoni, Ion acceleration by superintense laser-plasma interaction, Rev. Mod. Phys. **85**, 751 (2013).

[3] J. Fuchs, P. Antici, E. d'Humières, E. Lefebvre, M. Borghesi, E. Brambrink, C. A. Cecchetti, M. Kaluza, V. Malka, M. Manclossi, S. Meyroneinc, P. Mora, J. Schreiber, T. Toncian, H. Pėpin, and P. Audebert, Laser-driven proton scaling laws and new paths towards energy increase, Nat. Phys. **2**, 48 (2006).

[4] M. Roth, T. E. Cowan, M. H. Key, S. P. Hatchett, C. Brown, W. Fountain, J. Johnson, D. M. Pennington, R. A. Snavely, S. C. Wilks, K. Yasuike, H. Ruhl, F. Pegoraro, S. V. Bulanov, E. M. Campbell, M. D. Perry, and H. Powell, Fast ignition by intense laser-accelerated proton beams, Phys. Rev. Lett. **86**, 436 (2001).

[5] U. Linz and J. Alonso, What will it take for laser driven proton accelerators to be applied to tumor therapy, Phys. Rev. ST Accel. Beams **10**, 094801 (2007).

[6] S. V. Bulanov, T. Z. Esirkepov, V. S. Khoroshkov, A. V. Kuznetsov, and F. Pegoraro, Oncological hadrontherapy with laser ion accelerators, Phys. Lett. A **299**, 240 (2002).

[7] R. A. Snavely, M. H. Key, S. P. Hatchett, T. E. Cowan, M. Roth, T. W. Phillips, M. A. Stoyer, E. A. Henry, T. C. Sangster, M. S. Singh, S. C. Wilks, A. MacKinnon, A. Offenberger, D. M. Pennington, K. Yasuike, A. B. Langdon, B. F. Lasinski, J. Johnson, M. D. Perry, and E. M. Campbell, Intense high-energy proton beams from petawatt-laser irradiation of solids, Phys. Rev. Lett. **85**, 2945 (2000).

[8] L. L. Ji, B. F. Shen, X. M. Zhang, F. C. Wang, Z. Y. Jin, X. M. Li, M. Wen, and J. R. Cary, Generation monoenergetic heavy-ion bunches with laser-induced electrostatic shocks, Phys. Rev. Lett. **101**, 164802 (2008).

[9] A. X. Li, C. Y. Qin, H. Zhang, S. Li, L. L. Fan, Q. S. Wang, T. J. Xu, N. W. Wang, L. H. Yu, Y. Xu, Y. Q. Liu, C. Wang, X. L. Wang, Z. X. Zhang, X. Y. Liu, P. L. Bai, Z. B. Gan, X. B. Zhang, X. B. Wang, C. Fan, Y. J. Sun, Y. H. Tang, B. Yao, X. Y. Liang, Y. X. Leng, B. F. Shen, L. L. Ji, R. X. Li, and Z. Z. Xu, Acceleration of 60 MeV proton beams in the commissioning experiment of the SULF-10 PW laser, High Power Laser Sci. Eng. **10**, e26 (2022).

[10] D. Haberberger, S. Tochitsky, F. Fiuza, C. Gong, R. A. Fonseca, L. O. Silva, W. B. Mori, and C. Joshi, Collisionless shocks in laser-produced plasma generate monoenergetic high-energy proton beams, Nat. Phys. **8**, 95 (2012).

[11] F. Wagner, O. Deppert, C. Brabetz, P. Fiala, A. Kleinschmidt, P. Poth, V. A. Schanz, A. Tebartz, B. Zielbauer, M. Roth, T. Stöhlker, and V. Bagnoud, Maximum proton energy above 85 mev from the relativistic interaction of laser pulses with micrometer thick CH_2 targets, Phys. Rev. Lett. **116**, 205002 (2016).

[12] A. Higginson, R. J. Gray, M. King, R. J. Dance, S. D. R. Williamson, N. M. H. Butler, R. Wilson, R. Capdessus, C. Armstrong, J. S. Green, S. J. Hawkes, P. Martin, W. Q. Wei, S. R. Mirfayzi, X. H. Yuan, S. Kar, M. Borghesi, R. J. Clarke, D. Neely, and P. McKenna, Near-100 MeV protons via a laser-driven transparency-enhanced hybrid acceleration scheme, Nat. Commun. **9**, 724 (2018).

[13] N. P. Dover, M. Nishiuchi, H. Sakaki, K. Kondo, M. A. Alkhimova, A. Ya. Faenov, M. Hata, N. Iwata, H. Kiriyama, J. K. Koga, T. Miyahara, T. A. Pikuz, A. S. Pirozhkov, A. Sagisaka, Y. Sentoku, Y. Watanabe, M. Kando, and K. Kondo, Effect of small focus on electron heating and proton acceleration in ultrarelativistic laser-solid interactions, Phys. Rev. Lett. **124**, 084802 (2020).

[14] A. Macchi, S. Veghini, T. V. Liseykina, and F. Pegoraro, Radiation pressure acceleration of ultrathin foils, New J. Phys. **12**, 045013 (2010).

[15] S. S. Bulanov, E. Esarey, C. B. Schroeder, S. V. Bulanov, T. Zh. Esirkepov, M. Kando, F. Pegoraro, and W. P. Leemans, Enhancement of maximum attainable ion energy in the radiation pressure acceleration regime using a guiding structure, Phys. Rev. Lett. **114**, 105003 (2015).

[16] S. C. Wilks, A. B. Langdon, T. E. Cowan, M. Roth, M. Singh, S. Hatchett, M. H. Key, D. Pennington, A. MacKinnon, and R. A. Snavely, Energetic proton generation in ultra-intense laser-solid interactions, Phys Plamas. **8**, 542 (2001).

[17] T. Z. Esirkepov, M. Borghesi, S. V. Bulanov, G. Mourou, and T. Tajima, Highly efficient relativistic ion generation in the laser-piston regime, Phys. Rev. Lett. **92**, 175003 (2004).

[18] T. Z. Esirkepov, S. V. Bulanov, M. Kando, A. S. Pirozhkov, and A. G. Zhidkov, Boosted high-harmonics pulse from a double-sided relativistic mirror, Phys. Rev. Lett. **103**, 025002 (2009).

[19] A. Macchi, F. Cattani, T. V. Liseykina, and F. Cornolti, Laser acceleration of ion bunches at the front surface of overdense plasmas, Phys. Rev. Lett. **94**, 165003 (2005).

[20] A. P. L. Robinson, M. Zepf, S. Kar, R. G. Evans, and C. Bellei, Radiation pressure acceleration of thin foils with circularly polarized laser pulses, New J. Phys. **10**, 013021 (2008).

[21] X. Q. Yan, C. Lin, Z. M. Sheng, Z. Y. Guo, B. C. Liu, Y. R. Lu, J. X. Fang, and J. E. Chen, Generating high-current monoenergetic proton beams by a circularly polarized laser pulse in the phase-stable acceleration regime, Phys. Rev. Lett. **100**, 135003 (2008).

[22] A. Henig, S. Steinke, M. Schünrer, T. Sokollik, R. Hörlein, D. Kiefer, D. Jung, J. Schreiber, B. M. Hegelich, X. Q. Yan, J. Meyer-ter-Vehn, T. Tajima, P. V. Nickles, W. Sandner, and D. Habs, Radiation-pressure acceleration of ion beams driven by circularly polarized laser pulses, Phys. Rev. Lett. **103**, 245003 (2009).

[23] D. Jung, L. Yin, B. J. Albright, D. C. Gautier, R. Hörlein, D. Kiefer, A. Henig, R. Johnson, S. Letzring, S. Palaniyappan, R.

Shah, T. Shimada, X. Q. Yan, K. J. Bowers, T. Tajima, J. C. Fernández, D. Habs, and B. M. Hegelich, Monoenergetic ion beam generation by driving ion solitary waves with circularly polarized laser light, Phys. Rev. Lett. **107**, 115002 (2011).

[24] F. Dollar, C. Zulick, A. G. R. Thomas, V. Chvykov, J. Davis, G. Kalinchenko, T. Matsuoka, C. McGuffey, G. M. Petrov, L. Willingale, V. Yanovsky, A. Maksimchuk, and K. Krushelnick, Finite spot effects on radiation pressure acceleration from intense high-contrast laser interactions with thin targets, Phys. Rev. Lett. **108**, 175005 (2012).

[25] S. Kar, K. F. Kakolee, B. Qiao, A. Macchi, M. Cerchez, D. Doria, M. Geissler, P. McKenna, D. Neely, J. Osterholz, R. Prasad, K. Quinn, B. Ramakrishna, G. Sarri, O. Willi, X. Y. Yuan, M. Zepf, and M. Borghesi, Ion acceleration in multispecies targets driven by intense laser radiation pressure, Phys. Rev. Lett. **109**, 185006 (2012).

[26] I. J. Kim, K. H. Pae, I. I. W. Choi, C. L. Lee, H. T. Kim, H. Singhal, J. H. Sung, S. K. Lee, H. W. Lee, P. V. Nickles, T. M. Jeong, C. M. Kim, and C. H. Nam, Radiation pressure acceleration of protons to 93 MeV with circularly polarized petawatt laser pulses, Phys. Plasmas **23**, 070701 (2016).

[27] W. J. Ma, I. J. Kim, J. Q. Yu, II W. Choi, P. K. Singh, H. W. Lee, J. H. Sung, S. K. Lee, C. Lin, Q. Liao, J. G. Zhu, H. Y. Lu, B. Liu, H. Y. Wang, R. F. Xu, X. T. He, J. E. Chen, M. Zepf, J. Schreiber, X. Q. Yan, and C. H. Nam, Laser acceleration of highly energetic carbon ions using a double-layer target composed of slightly underdense plasma and ultrathin foil, Phys. Rev. Lett. **122**, 014803 (2019).

[28] A. Alejo, H. Ahmed, A. G. Krygier, R. Clarke, R. R. Freeman, J. Fuchs, A. Green, J. S. Green, D. Jung, A. Kleinschmidt, J. T. Morrison, Z. Najmudin, H. Nakamura, P. Norreys, M. Notley, M. Oliver, M. Roth, L. Vassura, M. Zepf, M. Borghesi, and S. Kar, Stabilized radiation pressure acceleration and neutron generation in ultrathin deuterated foils, Phys. Rev. Lett. **129**, 114801 (2022).

[29] Y. Kuramitsu, T. Minami, T. Hihara, K. Sakai, T. Nishimoto, S. Isayama, Y. T. Liao, K. T. Wu, W. Y. Woon, S. H. Chen, Y. L. Liu, S. M. He, C. Y. Su, M. Ota, S. Egashira, A. Morace, Y. Sakawa, Y. Abe, H. Habara, R. Kodama *et al.*, Robustness of large-area suspended graphene under interaction with intense laser, Sci. Rep. **12**, 2346 (2022).

[30] O. Lundh, F. Lindau, A. Persson, and C. G. Wahlström, Influence of shock waves on laser-driven proton acceleration, Phys. Rev. E **76**, 026404 (2007).

[31] C. Thaury, F. QuéRé, J. P. Geindre, A. Levy, T. Ceccotti, P. Monot, M. Bougeard, F. Réau, P. d'Oliveira, P. Audebert, R. Marjoribanks, and P. Martin, Plasma mirrors for ultrahigh-intensity optics, Nat. Phys. **3**, 424 (2007).

[32] F. Pegoraro and S. V. Bulanov, Photon bubbles and ion acceleration in a plasma dominated by the radiation pressure of an electromagnetic pulse, Phys. Rev. Lett. **99**, 065002 (2007).

[33] C. A. J. Palmer, J. Schreiber, S. R. Nagel, N. P. Dover, C. Bellei, F. N. Beg, S. Bott, R. J. Clarke, A. E. Dangor, S. M. Hassan, P. Hilz, D. Jung, S. Kneip, S. P. D. Mangles, K. L. Lancaster, A. Rehman, A. P. L. Robinson, C. Spindloe, J. Szerypo, M. Tatarakis *et al.*, Rayleigh-Taylor instability of an ultrathin foil accelerated by the radiation pressure of an intense laser, Phys. Rev. Lett. **108**, 225002 (2012).

[34] Y. Wan, I. A. Andriyash, W. Lu, W. B. Mori, and V. Malks, Effects of the transverse instability and wave breaking on the laser-driven thin foil acceleration, Phys. Rev. Lett. **125**, 104801 (2020).

[35] B. S. Paradkar and S. Krishnagopal, Electron heating in radiation-pressure-driven proton acceleration with a circularly polarized laser, Phys. Rev. E **93**, 023203 (2016).

[36] J. W. Yoon, Y. G. Kim, I. W. Choi, H. W. Lee, S. K. Lee, C. H. Nam, and Y. G. Kim, Realization of laser intensity over $10^{23}\mathrm{W/cm}^2$, Optica **8**, 630 (2021).

[37] S. V. Bulanov, T. Esirkepov, P. Migliozzi, F. Pegoraro, T. Tajima, and F. Terranova, Neutrino oscillation studies with laser-driven beam dump facilities, Nucl. Instrum. Methods Phys. Res., Sect. A **540**, 25 (2005).

[38] S. M. Weng, M. Murakami, P. Mulser, and Z. M. Sheng, Ultra-intense laser pulse propagation in plasmas: From classic hole-boring to incomplete hole-boring with relativistic transparency, New J. Phys. **14**, 063026 (2012).

[39] M. Grech, S. Skupin, A. Diaw, T. Schlegel, and V. T. Tikhonchuk, Energy dispersion in radiation pressure accelerated ion beams, New J. Phys. **13**, 123003 (2011).

[40] A. P. L. Robinson, P. Gibbon, M. Zepf, S. Kar, R. G. Evans, and C. Bellei, Relativistically correct hole-boring and ion acceleration by circularly polarized laser pulses, Plasma Phys. Control. Fusion **51**, 024004 (2009).

[41] A. Pukhov and J. Meyer-ter-Vehn, Laser hole boring into overdense plasma and relativistic electron currents for fast ignition of ICF targets, Phys. Rev. Lett. **69**, 3052 (1992).

[42] T. P. Yu, A. Pukhov, G. Shvets, and M. Chen, Stable laser-driven proton beam acceleration from a two-ion-species ultrathin foil, Phys. Rev. Lett. **105**, 065002 (2010).

[43] B. Qiao, M. Zepf, M. Borghesi, and M. Geissler, Stable GeV ion-beam acceleration from thin foils by circularly polarized laser pulses, Phys. Rev. Lett. **102**, 145002 (2009).

[44] M. Chen, A. Pukhov, T. P. Yu, and Z. M. Sheng, Enhanced collimated GeV monoenergetic ion acceleration from a shaped foil target irradiated by a circularly polarized laser pulse, Phys. Rev. Lett. **103**, 024801 (2009).

[45] T. D. Arber, K. Bennett, C. S. Brady, A. L. Douglas, M. G. Ramsay, N. J. Sircombe, P. Gillies, R. G. Evans, H. Schmitz, A. R. Bell, and C. P. Ridgers, Contemporary particle-in-cell approach to laser-plasma modelling, Plasma Phys. Control. Fusion **57**, 113001 (2015).

[46] See Supplemental Material at http://link.aps.org/supplemental/10.1103/PhysRevE.109.015208 for the additional analysis and simulation results and it includes four notes and five figures. In Note 1, we introduce the method of counting the efficient target thickness in simulations. The energy conversion efficiency and the number of accelerated protons are analyzed in Note 2. The influence of the QED effects on the energy peaks of proton beams and the energy conversion of generated gamma photons, electrons and protons are presented in Note 3. The proton acceleration from Lithium Hydride (LiH) is investigated in Note 4.

[47] M. Liu, S. M. Weng, H. C. Wang, M. Chen, Q. Zhao, Z. M. Sheng, M. Q. He, Y. T. Li, J. Zhang, Efficient injection of radiation-pressure-accelerated sub-relativistic protons into laser wakefield acceleration based on 10 PW lasers, Phys. Plasmas. **25**, 063103 (2018).

[48] S. V. Bulanov, T. Zh. Esirkepov, M. Kando, F. Pegorraro, S. S. Bulanov, C. G. R. Geddes, C. B. Schroeder, E. Esarey, and W. P. Leemans, Ion acceleration from thin foil and extended plasma

targets by slow electromagnetic wave and related ion-ion beam instability, Phys. Plasmas. **19**, 103105 (2012).

[49] K. A. Tanaka, K. M. Spohr, D. L. Balabanski, S. Balascuta, L. Capponi, M. O. Cernaianu, M. Cuciuc, A. Cucoanes, I. Dancus, A. Dhal, B. Diaconescu, D. Doria, P. Ghenuche, D. G. Ghita, S. Kisyov, V. Nastasa, J. F. Ong, F. Rotaru, D. Sangwan, P. A. Söderström, D. Stutman *et al.*, Current status and highlights of the ELI-NP research program, Matter Radiat. Extremes **5**, 024402 (2020).

[50] Z. Gan, L. Yu, C. Wang, Y. Q. Liu, Y. Xu, W. Q. Li, S. Li, L. P. Yu, X. L. Wang, X. Y. Liu, J. C. Chen, Y. J. Peng, L. Xu, B. Yao, X. B. Zhang, L. R. Chen, Y. H. Tang, X. B. Wang, D. J. Yin, X. Y. Liang, Y. X. Leng, R. X. Li, and Z. Z. Xu, *The Shanghai superintense ultrafast laser facility (SULF) project in Progress in Ultrafast Intense Laser Science XVI* (Springer International Publishing, Cham, 2021), p. 199.

[51] C. Radier, O. Chalus, M. Charbonneau, S. Thambirajah, G. Deschamps, S. David, J. Barbe, E. Etter, G. Matras, S. Ricaud, V. Leroux, C. Richard, F. Lureau, A. Baleanu, R. Banici, A. Gradinariu, C. Caldararu, C. Capiteanu, A. Naziru, B. Diaconescu, V. Iancu, R. Dabu, D. Ursescu, I. Dancus, C. A. Ur, K. A. Tanaka, and N. V. Zamfir, 10 PW peak power femtosecond laser pulses at ELI-NP, High Power Laser Sci. Eng. **10**, e21 (2022).

[52] V. B. Berestetskii, E. M. Lifshitz, and L. P. Pitaevskii, *Quantum Electrodynamics* (Elsevier Butterworth-Heinemann, Oxford, 1982).

[53] V. I. Ritus, Quantum effects of the interaction of elementary particles with an intense electromagnetic field, J. Sov. Laser Res. **6**, 497 (1985).

[54] V. N. Baier, V. Katkov, and V. M. Strakhovenko, *Electromagnetic Processes at High Energies in Oriented Single Crystals* (World Scientific, Singapore, 1998).

[55] A. Di Piazza, C. Müller, K. Z. Hatsagortsyan, and C. H. Keitel, Extremely high-intensity laser interactions with fundamental quantum systems, Rev. Mod. Phys. **84**, 1177 (2012).

[56] M. Tamburini, F. Pegoraro, A. Di Piazza, C. H. Keitel, and A. Macchi, Radiation reaction effects on radiation pressure acceleration, New J. Phys. **12**, 123005 (2010).

[57] C. P. Ridgers, C. S. Brady, R. Duclous, J. G. Kirk, K. Bennett, T. D. Arber, A. P. L. Robinson, and A. R. Bell, Dense elecron-positron plasmas and ultraintense γ rays from laser-irradiated solids, Phys. Rev. Lett. **108**, 165006 (2012).

[58] C. S. Brady, C. P. Ridgers, T. D. Arber, A. R. Bell, and J. G. Kirk, Laser absorption in relativistically underdense plasmas by synchrotron radiation, Phys. Rev. Lett. **109**, 245006 (2012).

[59] W. M. Wang, P. Gibbon, Z. M. Sheng, Y. T. Li, and J. Zhang, Laser opacity in underdense preplasma of solid targets due to quantum electrodynamics effects, Phys. Rev. E **96**, 013201 (2017).

[60] J. Davis and G. M. Petrov, Generation of GeV ion bunches from high-intensity laser-target interactions, Phys. Plasmas **16**, 023105 (2009).